minerals

MDPI

Article

Sulfate Kinetics and Adsorption Studies on a Zeolite/Polyammonium Cation Composite for Environmental Remediation

Carmen Pizarro [1,2,*], Mauricio Escudey [1,2], Camila Bravo [1,2], Manuel Gacitua [1,2] and Lynda Pavez [1,2]

[1] Facultad de Química y Biología, Universidad de Santiago de Chile, Av. L. B. O'Higgins, 3363, Santiago 7254758, Chile; mauricio.escudey@usach.cl (M.E.); camila.bravog@usach.cl (C.B.); manuel.gacitua@usach.cl (M.G.); lynda.pavez@usach.cl (L.P.)

[2] Center for the Development of Nanoscience and Nanotechnology (CEDENNA), Santiago 9170124, Chile

* Correspondence: carmen.pizarro@usach.cl

Abstract: Sulfide mineral mining produces highly sulfate-contaminated wastewater which needs to be treated before disposal. A composite material was made from natural zeolite (NZ) and Superfloc® SC-581, a polyammonium cationic polymer. The resulting modified zeolite (MZ) demonstrated improved capacity for sulfate abatement from wastewater compared to NZ. Above pH 4.0, MZ retained positive surface charge while NZ remained negative. The effect of the ionic strength on the adsorption process was evaluated. Sulfate adsorption capacity was assessed and revealed MZ to be superior to NZ in all cases. Adsorption kinetics reached equilibrium after 10–12 h, with MZ adsorption being twice that of NZ; data fitted a pseudo-second order kinetic model. Adsorption isotherms reflected the high capacity of MZ for sulfate adsorption with maximum of 3.1 mg g^{-1}, while NZ only achieved 1.5 mg g^{-1}. The process corresponds to heterogeneous partially reversible adsorption of ionic species over the solid adsorbent. Langmuir–Freundlich parameters revealed that adsorption over MZ corresponds to an interaction eight times stronger than that on NZ. The sulfate adsorption pattern changes with ionic strength. Taken together, the composite formed between natural zeolite and polyammonium represents an adsorbent that maintains the adsorption capacity of zeolite and proves suitable for anionic species removal. Further prospect considers the testing of the composite with other anionic pollutants (arsenate, phosphate, perchlorate, etc.)

Keywords: cationic polymer; surface modified zeolite; sulfate adsorption; ionic strength

Citation: Pizarro, C.; Escudey, M.; Bravo, C.; Gacitua, M.; Pavez, L. Sulfate Kinetics and Adsorption Studies on a Zeolite/Polyammonium Cation Composite for Environmental Remediation. *Minerals* **2021**, *11*, 180. https://doi.org/10.3390/min11020180

Academic Editor: Veronica Mpode Ngole-Jeme

Received: 22 December 2020

Accepted: 4 February 2021

Published: 9 February 2021

1. Introduction

Mining activities worldwide represent an important economic activity, with reported annual incomes near USD 600 billion during 2017 from the top 40 mining companies [1]. Mining has inherent environmental consequences, as intense mineral processing produces large volumes of industrial waste [2,3]. Mineral extraction from deposits, metal purification with leaching, and production of smelter wastes result in wastewater of varied composition depending on the source and local geological composition. Several reports indicate that typical wastewater from Chilean mines [4] contains high levels of sulfate (ca. 14,400 ppm). The release of sulfate-polluted wastewaters into natural water bodies presents significant environmental consequences [5] such as sulfide liberation through microorganism anaerobic respiration from sulfates [6] and eutrophication [7]. Therefore, treatment of wastewater generated from mining activities is critical for sustainable development [8–10].

Sulfate abatement from wastewater remains a technological challenge. Commonly employed methods include chemical precipitation [11], biological treatment [12] and adsorption techniques [13,14]. Chemical precipitation, biological or adsorption treatments are associated with high installation and operational costs that may contain harmful substances with greater health and environmental risks than sulfate [15]. A suitable sulfate

remediation method would ideally involve naturally abundant, low-cost materials able to reduce water sulfate, but with environmentally friendly products.

Notably, Chile has enormous deposits of zeolite, a renowned adsorbent material used in a range of applications from adsorption to catalysis [16]. Natural zeolite is an aluminosilicate mineral that typically presents permanent negative surface charge due to isomorphic substitution of its Si^{4+} ions with Al^{3+} [17]. Due to its high cation exchange ability and molecular sieve properties, natural zeolite (NZ) has been widely used as a metal adsorbent. [18,19]. The adsorption characteristic of zeolites is influenced by their high specific surface area, with active sites that have the capability to adsorb a large variety of compounds. Some authors have applied zeolite to remove ammonium from wastewater, recovering nitrogen nutrients and preventing eutrophication of natural water bodies [20–22]. These properties can be modulated by chemical treatments to promote anion adsorption efficiency of natural clays [23–27]. For instance, cationic surfactants [13,28–30] polycationic chitosan [31], and cationic polyacrylamide [32] can be used for this purpose. Due to typical cationic surfactant behavior, these compounds are adsorbed over zeolite through the positively charged head, leaving the non-polar tails in solution. Then, a second layer of cationic surfactant deposits through their lipophilic tails, leaving the positively charged head in contact with the bulk solution and free to adsorb anions, as explained by Kamble et al. [33].

In this work, we describe for the first time the preparation of a composite made from Chilean natural zeolite samples and Superfloc® SC-581, a polyamine polycation (or cationic polymer) of commercial origin. Superfloc® SC-581 is a co-polymer between neutral and cationic polyacrylamide commonly used as an organic flocculant for wastewater treatment in mining activities [34,35]. The modified zeolite (MZ) composite is assayed as adsorbent for sulfates in a synthetic sulfate-polluted water solution. Surface charge analysis and sulfate adsorption experiments were performed to optimize the modification of NZ and assess the sulfate affinity of the resulting composite. Since mining wastewater contains a high ionic concentration, the ionic strength effect [36,37] on adsorption is also studied. Finally, adsorption kinetics and isotherms were performed and modeled to evaluate the adsorption capabilities of the composite material.

2. Materials and Methods

2.1. Materials

Natural zeolite (NZ) samples were obtained from a source located in the central-south zone of Chile (geographical coordinates 36°16′S 71°40′W). Before adsorption studies, natural zeolite was characterized to check its suitability as adsorbent material. Properties of natural zeolite (NZ) are presented in Table 1.

Table 1. Natural zeolite characterization.

pH (zeolite: water = 1.0:2.5)	6.6 ± 0.1
Total specific surface area TSSA ($m^2\ g^{-1}$)	74 ± 6
External surface area BET ($m^2\ g^{-1}$)	42 ± 1
Pore size	2.6 × 5.7 and 6.5 × 7.5 Å
Isoelectric point (IEP)	3.1 ± 0.1
General Formula (XRD analysis)	$Ca_{3.4}Al_{7.4}Si_{40.6}O_{96}(H_2O)_{31}$
Particle size distribution	
Size fraction (μm)	%
<2	20.2 ± 0.1
2–20	54.4 ± 1.5
20–53	21.9 ± 1.1
53–2000	3.5 ± 0.3

Several characteristics of NZ reflect its suitability to environmental remediation applications. First, the pH value of NZ is close to neutral (6.6), suggesting that the application of

this mineral in remediation technologies would not result in major pH shifts to water bodies. Moreover, the Si/Al ratio as determined though X-Ray diffractometry (XRD) analysis corresponds to a medium level (5.5) according to the Van Bekkum et al. [38] proposed scale, indicating considerable isomorphic substitution of Si^{4+} atoms by Al^{3+} to produce a mineral with a permanent negative surface charge. According to the isoelectric point (IEP) value, this negative surface charge is developed from a relatively low pH (3.1). This is important for synthesizing the composite: SC-581 is a permanent positive charge water-stable polymer (or polycation); thus, formation of the composite between the negatively charged NZ and SC-581 is feasible simply through electrostatic attraction. XRD analysis reveals that NZ corresponds to a rehydrated mordenite-type zeolite that possesses exchangeable calcium in its structure as represented by its general formula, $Ca_{3.4}Al_{7.4}Si_{40.6}O_{96}(H_2O)_{31}$ [39]. Finally, approximately 75% of NZ is 20 μm or less in size. This property is promising, since particles in this size range present the highest adsorption capacities due to their elevated contact surface [39–41]. Collectively, these characteristics make NZ a suitable starting material for further development of composites to be used for adsorption of anionic species such as sulfates. Then, modified zeolite was prepared by combination with SC-581.

NZ samples were modified with Kemira Superfloc C-581® (SC-581), a polycation with high relative molecular weight, melting point at −18 °C, and a density of 1.14–1.18 g mL^{-1} at 25 °C [34,35,42]. Other reagents are KCl (99.0%, Merck), HCl (37%, Merck), NaOH (>98% Aldrich), ethanol (96% Merck), NaCl (>99% Aldrich), glycerol (>99.5% Aldrich) and $BaCl_2$ (99.99% Aldrich). Double distilled water (18 MΩ cm^{-1}) was employed in all experiments.

2.2. Methods

The pH was measured in the supernatant of the solid: double distilled water in a mass ratio of 1.0:2.5 after 2 h of continuous orbital stirring and 3 h of rest.

The total specific surface area (TSSA) was determined gravimetrically, applying the ethylene glycol monoethyl ether (EGME) technique, proposed by Carter et al. [43] to determine the TSSA of the soils.

External surface area was determined using a 0.3 g sample. The sample was firstly degassed and adsorption–desorption isotherms of N_2 at −195 °C (77 K) were acquired, changing the relative pressure (P/Po) of the gas and recording the volume adsorbed on the solid's surface. The specific surface area was calculated from the amount of N_2 adsorbed employing the Brunauer–Emmett–Teller or BET equation [44].

The silicon/aluminum (Si/Al) ratio and the chemical formula of NZ was determined by X-ray diffraction experiments run on a Siemens D5000 X-Ray diffractometer (Germany) with Bragg-Brentano geometry and an X-ray tube with copper anode (wavelength 1.54 Å). Data analysis was carried out using the Direct Plus EVA 15 (2009) database PDF-2 (Powder Diffraction File, 2003). The particle size distribution was measured for each adsorbent through methodology based on Stoke's law relating sedimentation speed with particle diameter [45]. Exchangeable cations were determined for NZ samples. After hominization with KCl 0.05 mol L^{-1}, samples were centrifuged and the quantity of Ca and Mg at the supernatant were determined through Inductively Coupled Plasma Atomic Emission Spectroscopy analysis.

Isoelectric point (IEP) values were determined by micro-electrophoresis directly on NZ and MZ particles with reported particle size distribution. Electrophoretic mobilities were measured with a zeta meter ZM-77 apparatus (USA). Dilute dispersions of adsorbents (0.05 g L^{-1}) were prepared in 10^{-3} mol L^{-1} of KCl and pH was adjusted with 10^{-2} mol L^{-1} of HCl or NaOH. The mobilities were averaged and the zeta potential was calculated using the Helmholtz–Smoluchowski equation [46]. Experimental points obtained showed a 10% coefficient of variation in zeta potential.

2.3. Modification Process

Zeolite was firstly washed by adding 1 g in 50 mL centrifuge tubes with 25 mL of double distilled water. The mix was orbitally agitated at 300 rpm for 30 min and centrifuged

at 6000 rpm for 5 min and the supernatant was eliminated. This washing process was repeted three times. The washed zeolite was then homoionized. Homoionization of the zeolite was identical to the wash steps but used 0.1 mol L^{-1} of KCl solution. After the third elimination of supernatan, the homoionized zeolite was freeze-dried at low presure.

Modified zeolite was prepared by placing 1 g of homoionized NZ in 50 mL centrifuge tubes with 25 mL of SC-581 at a specific concentration (0.1 to 12.0 mg L^{-1}) followed by orbital agitation for 3 h. The mixture was then separated through centrifugation (6000 rpm per 10 min). The supernatant was discarded, and the solids were stored for further analyses, including measurement of pH, surface area, particle size distribution, zeta-potential, and isoelectric point.

2.4. Adsorption

2.4.1. Ionic Strength Effect

Adsorption isotherms of sulfate onto KCl-homoionized zeolite were obtained through batch experiments at different ionic strengths using 0.001, 0.050 and 0.100 mol L^{-1} of KCl. The concentration of sulfate at equilibrium ranged from 100 to 500 mg L^{-1}. Sulfate in solution at equilibrium was determined through turbidimetry.

2.4.2. Adsorption Kinetics

In 50 mL polypropylene centrifuge tubes, 20 mL of 1000 ppm SO_4^{2-} solution in 0.05 mol L^{-1} of KCl was mixed with a 5% *w*/*v* solid ratio of adsorbent (NZ or MZ). The tubes were stirred (300 rpm) in a reciprocating shaker using time intervals of 1, 3, 6, 9, 12, 16, 20 and 24 h. At the end of each time interval, the tubes were centrifuged at 6000 rpm for 10 min. The supernatant was filtered and used for the quantification of sulfate ions using the turbidimetric method. The experimental results were used to calculate the amount of adsorbed sulfate as a function of time, C_t (mg g^{-1}), determined by mass balance, according to the equation:

$$C_t = \frac{(C_{S0} - C_{St})}{m} V \quad (1)$$

where C_{S0} and C_{St} are the sulfate initial and final concentrations (mg L^{-1}), respectively, in the supernatant; V (L) is the total volume of solution in the tubes; and m is the mass (g) of adsorbent employed. Adsorption kinetic data were fitted employing pseudo-first and -second order models. The pseudo-first order kinetic model assumes that a solute ion is adsorbed on a surface site of the adsorbent [47,48]. The integrated form of the pseudo-first order kinetic rate equation is:

$$\log(C_m - C_t) = \log C_{m\text{-}cal} - \frac{k_1 t}{2.303} \quad (2)$$

where C_t is the adsorbed quantity at any time (t), C_m is the maximum experimental adsorbed amount (obtained from the kinetic curve), k_1 is a combination of the adsorption and the desorption rate constants, and $C_{m\text{-}cal}$ corresponds to the maximum adsorbed amount as determined by the application of the model. $C_{m\text{-}cal}$ and C_m will agree if the model succeeds in giving a perfect description of the experimental data.

The pseudo-second order kinetic model postulates that solute adsorption occurs on two available surface sites of the adsorbent. The integrated form of the pseudo-second order kinetic rate equation is [47–49]:

$$\frac{t}{C_t} = \frac{1}{(C_{m\text{-}cal})^2 k_2} + \frac{1}{C_{m\text{-}cal}} t \quad (3)$$

The observed rate constant of the pseudo-second order equation (k_2) is a complex function of the initial solute concentration. This linear plot may be described as a chemisorption process.

2.4.3. Adsorption Isotherms

Experimental points were obtained in a similar manner to those for adsorption kinetics but with the sulfate concentration ranging from to 0 to 700 mg L^{-1} of SO_4^{2-} in 0.05 mol L^{-1} of KCl. Quantification and mass balance were also made the same way. Adsorption isotherms data were fitted using Freundlich [50] Langmuir [47], and the Langmuir–Freundlich [51,52] adsorption models. The Freundlich model does not have a mechanistic interpretation; it only represents an empirical approach to predict the species distribution between a solid/solution phase, and described by:

$$C_s = K_F (C_{Se})^{\frac{1}{n_{fads}}} \quad (4)$$

where K_F and n_{fads} are adjustable parameters with $0 < 1/n_{fads} < 1$ (usually), C_s is the concentration of adsorbed species (mg g^{-1}), and C_{Se} is the concentration in the supernatant solution (mg L^{-1}). K_F corresponds to the empirical Freundlich adsorption coefficient and n_{fads} is a linearity factor.

The Langmuir model assumes that adsorption of the solute on a solid takes place through formation of a monolayer. It considers ideal solutions where adsorption is independent of the coverage of the surface; the sites on which the adsorption takes place are uniformly distributed on the adsorbent surface; energy due to the interaction is equal at all the interaction sites; and a fixed number of exchange sites exists. The Langmuir model is applicable to L-type isotherms, characterized by a high affinity between adsorbate and adsorbent, commonly implying a chemical adsorption with the formation of inner sphere complexes [53]. The Langmuir model is described by:

$$C_s = C_{m\text{-}cal} \frac{K_L C_{Se}}{1 + K_L C_{Se}} \quad (5)$$

where C_s and C_{Se} have the same meaning as in the Freundlich model, $C_{m\text{-}cal}$ is the maximum adsorption capacity (mg g^{-1}) calculated by the model and K_L is the empirical affinity Langmuir coefficient (L mg^{-1}).

The combined Langmuir–Freundlich model (Sips model) [54] is expressed by:

$$C_s = \frac{C_{m\text{-}cal} (C_{Se})^n}{K_d + (C_{Se})^n} \quad (6)$$

where K_d is the apparent equilibrium affinity constant for heterogeneous solids, which includes k_2/k_1 contributions; k_1 is the adsorption rate constant; k_2 is the dissociation rate constant; and "n" is the Langmuir–Freundlich heterogeneity parameter. This "n" value can also be employed as an empirical coefficient, representing the type and extent of cooperativity present in the binding interaction [52].

2.4.4. Turbidimetric Analysis of Sulfate

1 mL of sulfate-containing samples was placed in an Eppendorf tube with 0.05 mL of conditioning solution (prepared by mixing 30 mL of concentrated HCl, 300 mL of double distilled water, 100 mL of ethanol 96%, 75 g of NaCl, and 50 mL of glycerol). Then 0.01 g of $BaCl_2$ crystals were added and the mix was stirred continuously for 1 min. Immediately after that, sample was transferred into a cuvette and absorbance was measured at 500 nm of wavelength [55] using a Thermo Electron Spectronic Helios Alpha Beta UV-Visible double beam spectrophotometer (USA). In parallel, a calibration curve (sulfate concentration 0–40 mg mL^{-1}) was prepared following same procedure as described for samples. Sulfate concentration was determined using the calibration curve equation [55].

3. Results and Discussion

3.1. Preparation of Modified Zeolite

Modified zeolite (MZ) synthesis was optimized through measurement of zeta potential across increasing quantities of SC-581. This optimization is shown in Figure 1. pH values for each experimental point were on average 6.6 ± 0.1.

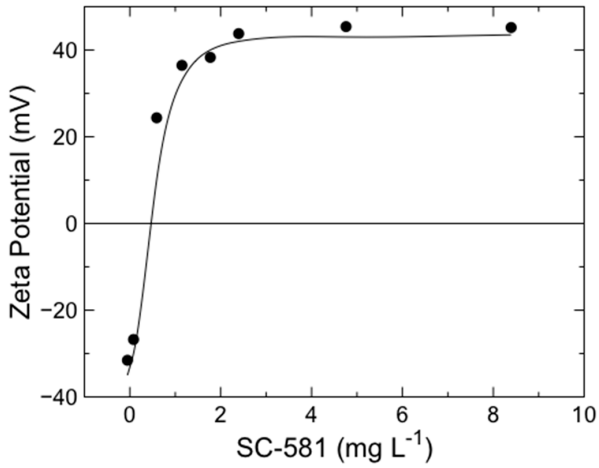

Figure 1. Zeta potential variation during modified zeolite (MZ) synthesis with increasing SC-581 concentration.

Optimization of MZ synthesis revealed that low amounts of polycation effectively change the surface charge of NZ. As shown in Figure 1, 25 mL of a 0.6 mg L^{-1} of SC-581 effectively neutralizes the negative charge of 1 g of NZ. As zeta potential reached a plateau of 45.2 mV after the addition of 4.8 mg L^{-1} of the polycation, this concentration was employed for preparation of the composite between NZ and SC-581 to produce MZ. IEP determination for NZ and MZ is presented in Figure 2.

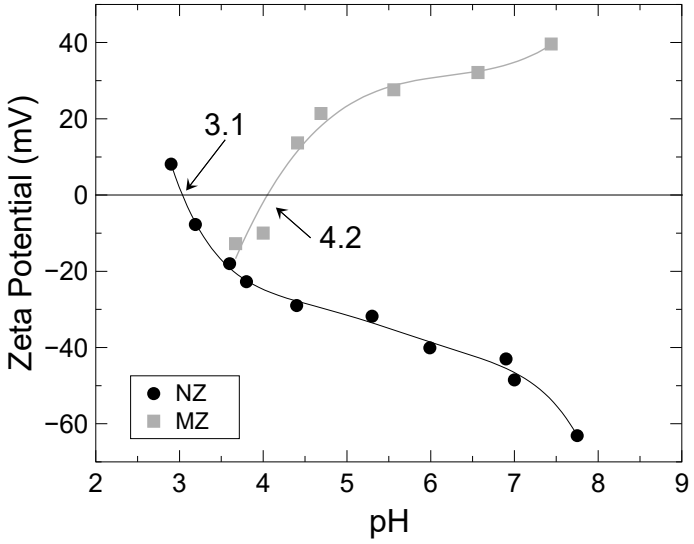

Figure 2. Determination of isoelectric point of adsorbents. Zeta potential was measured across increasing pH.

At first glance, these adsorbents exhibit marked variation in the curve of the slope. NZ develops negative surface charge at pH values greater than 3.1 (NZ isoelectric point), while MZ displays positive surface charge from pH values greater than its IEP (4.2). Interestingly, the curve for IEP determination of MZ always maintains a positive slope. When determining IEP through electrophoretic mobility studies, pH elevation typically

potentiates negative charge over adsorbents. However, if multivalent cationic species (divalent: M^{2+}; polyvalent: M^{n+}, with $n > 1$) are abundant, the formation of surface complexes may result in the development of positive charge with increasing pH. Such behavior has been observed before for different systems. Escudey and Gil-Llambias [56] reported positive slope curves when determining the IEP of MoO_3/γ-Al_2O_3 catalyst if divalent cations (Ca^{2+} and Ba^{2+}) were present in the background electrolyte. More recently, Arancibia-Miranda et al. [57] studied the effect of cations on the IEP of imogolite samples, observing a positive slope for zeta potential vs. pH curves in the presence of divalent cations (Ca^{2+} and Mg^{2+}). In the interaction of SC-581 with NZ, the polymer acts analogously to multivalent cations. SC-581 consists of a co-polymer between neutral and cationic polyacrylamide. Smets and Hesbain [58] studied the effect of pH on the structure and stability of the polyacrylamide polymer, proving that its structure was extremely sensitive to low pH conditions. This work demonstrated that the polymer breaks down into its monomeric components at pH values less than 5.0, with lower pH values accelerating this process. Moreover, the product sheet for Superfloc C-581 [34,35] states the adequate working pH window to be 4.0–7.0. Indeed, at pH values below 4.0, SC-581 polycation structures break down into their components (2-chloromethyl oxirane, ethane-1,2-diamine and N-methylmethanamine) [59] which may still form multivalent oligomeric species. These polymer fragments may stablish surface complexes over the NZ surface, elevating surface charge to positive values with increasing pH. Therefore, sulfate adsorption experiments should be carried out at pH values $\geq$ 4.5 to ascertain that zeolite remains effectively modified by the polycation. In this pH range, NZ and MZ adsorbents should present negative and positive surface charge, respectively (Figure 2). Regarding external surface area (BET) and pore size for the composite, it can be presumed that was maintained nearly the same as those for the natural zeolite since Dickson et al. (2020) [30] reported that zeolite containing similar Si/Al ratios did not modify these properties greatly after being modified with cationic surfactant hexadecyltrimethylammonium bromide. Also, if the hydrated radii of sulfate are reported to be 3.79 Å [60], then the interaction with the adsorbents may take place in the external surface or inside the adsorbent pores; sulfate would probably lose its solvated water molecules before. Finally, regarding the interaction between sulfate and the composite, according to zeta potential vs. pH diagrams at pH values of 4.2 or higher, the positive charge of the composite ensures the electrostatic interaction between sulfate and the solid, explaining in part the interaction.

3.2. Adsorption

The effect of ionic strength on sulfate adsorption is presented in Figure 3.

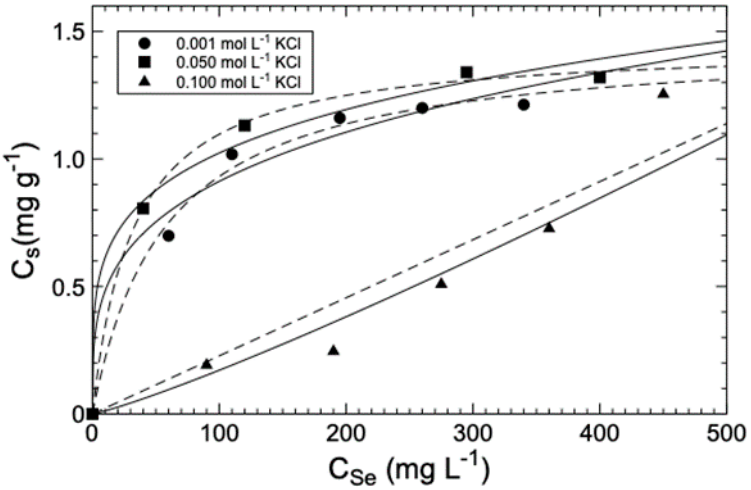

Figure 3. Effect of ionic strength (expressed as KCl concentration) on adsorption isotherms. Freundlich and Langmuir model adjustment corresponds to straight and dashed lines, respectively.

Fitted curves for ionic strength of 0.001 and 0.050 mol L^{-1} of KCl are quite similar. Both curves fit the Langmuir adsorption model well with a maximum of adsorption ($C_{m\text{-}cal}$) of 1.421 and 1.439 mg g^{-1}, respectively. Interestingly, increasing the KCl concentration to 0.100 mol L^{-1} changed the adsorption isotherm curve pattern from L-type to S-type. The L-type isotherm curve describes a high-affinity adsorption between sulfate and NZ, indicating chemisorption, while the S-type isotherm describes an interaction between sulfate species over the NZ and/or the adsorption of sulfate on NZ through solution ligands [47]. The difference in the adsorption curve pattern indicates that the sulfate adsorption process is modified as ionic strength increases, thus, maintaining low concentrations of KCl would be preferential to avoid shifting the adsorption mechanism. This could be explained by the formation of outer sphere complexes, in which electrostatic forces are responsible for adsorption. Therefore, these complexes may be easily affected by variations in ionic strength [61,62]. Consequently, it is possible that at KCl concentrations higher than 0.050 mol L^{-1}, chloride ions begin to compete with sulfate for adsorption sites and consequently reduce sulfate adsorption.

3.3. Adsorption Kinetics

Adsorption kinetics experiments determine both adsorption rates, the time needed to reach equilibrium, the type of adsorption taking place as well as the route and mechanism of the reaction [63]. Results from adsorption kinetics experiments for sulfate on NZ and MZ are in Figure 4.

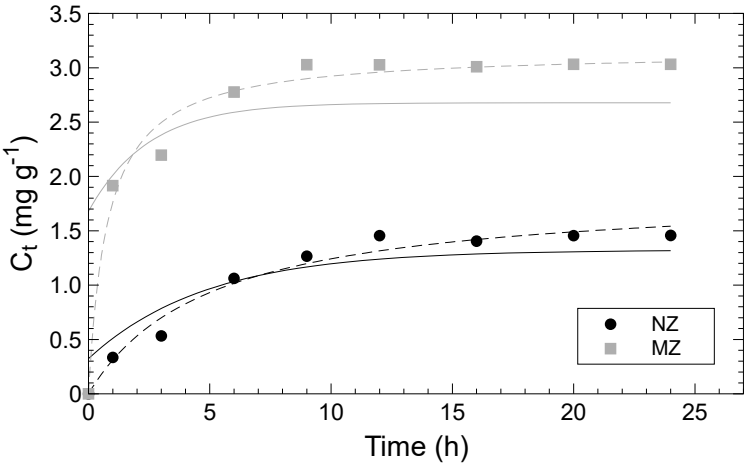

Figure 4. Sulfate adsorption kinetics. Key: Experimental data (points), Pseudo-first (straight) and -second order (dashed) kinetic model adjustments. NZ: natural zeolite; MZ: modified zeolite.

Adsorbents became saturated after 10–12 h of equilibration time (Figure 4). Analyzing the plateaus, maximum adsorption capacity for kinetic studies on MZ is almost 2.2 times higher than on NZ. This preliminary result indicates that SC-581 effectively modified the surface of NZ to enhance sulfate adsorption capacity. Fitting parameters for pseudo-first- and pseudo-second order kinetic models are presented in Table 2.

Table 2. Kinetics model fit parameters.

Pseudo 1st Order Model		**NZ**	**MZ**
C_m	(mg g^{-1})	1.32	2.68
k_1	(h^{-1})	0.21	0.41
R^2		0.88	0.57
Pseudo 2nd Order Model		**NZ**	**MZ**
C_m	(mg g^{-1})	1.86	3.16
k_2	(g mg^{-1} h^{-1})	0.11	0.40
R^2		0.98	0.98

For both adsorbents, the pseudo-second order model better fits the kinetic data according to the correlation coefficient (R^2). Other authors have made the same observation for sulfate adsorption on modified aluminosilicate-based adsorbents with increased positive surface charge, resulting in the enhancement of their anion adsorption capacities. Chen and Liu [64] determined pseudo-second order kinetics when studying sulfate adsorption over natural zeolite modified with cationic surfactant cetyltrimethylammonium bromide (CTAB), reaching saturation after only 2 h. Moreover, Matusik [65] determined pseudo-second order kinetics for the adsorption of sulfate, nitrate, orthophosphate, and arsenate onto N-methyl-diethanolamine-grafted kaolinite samples, achieving equilibrium time swiftly after 20 min. In the present work, adjustment parameters reveal that MZ adsorbs sulfate from solution 3.7 times faster (k_2) and displays 1.7 times greater adsorption capacity (C_m) compared to NZ. Therefore, SC-581 modification of NZ effectively increases adsorption rate of sulfate. To further understand adsorption dynamics, we produced adsorption isotherms by exposing the adsorbents to different concentrations of sulfate until equilibrium is reached (after 12 h). The adsorption isotherms are in Figure 5.

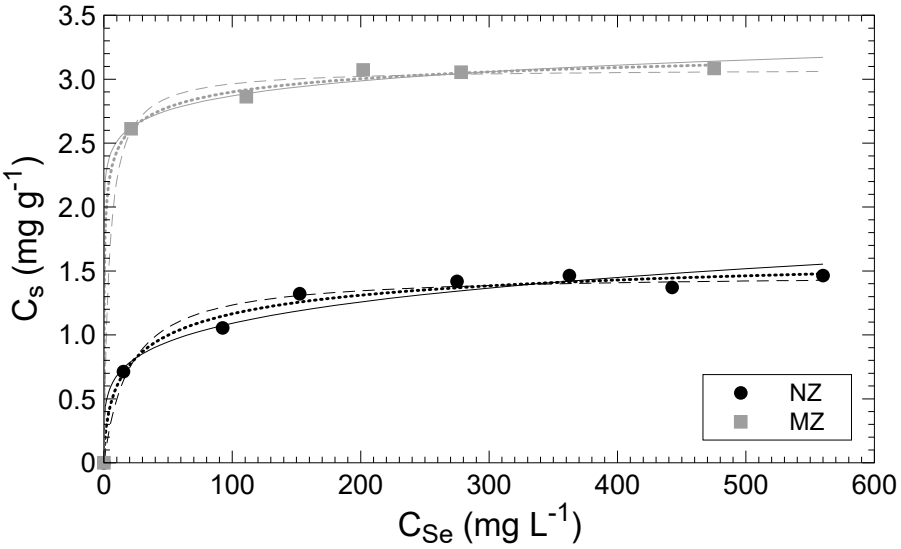

Figure 5. Sulfate adsorption isotherms. Key: Experimental data (points), Freundlich (straight), Langmuir (dashed) and Langmuir-Freundlich (doted) model adjustments.

As Figure 5 illustrates, the amount of adsorbed sulfate, C_s, increases rapidly when the concentration of sulfate at equilibrium, C_{Se}, increases. As experiments were carried out at pH 4.8 ± 0.1, these data indicate that the composite structure of MZ was not threatened after the adsorption process. The isotherm shape of NZ resembles L-type isotherms, which represent a relatively strong adsorption interaction [53]. On the other hand, the MZ shape is more similar to H-type isotherms, implying a stronger interaction between analyte and adsorbents [53]. Experimental sulfate maximum adsorption capacity on NZ and MZ over is about 1.5 and 3.1 mg g^{-1}, respectively. Therefore, as expected from the IEP and adsorption kinetic data, sulfate adsorption capacities increased after modification with SC-581. Comparable results have been attained by other authors, including 2.5 mg g^{-1} of sulfate maximum adsorption on hexadecyltrimethylammonium-modified zeolite [66]. Moreover, maximum sulfate adsorption of 5.02 mg g^{-1} was reported for methyl-diethanolamine-grafted kaolinite samples by Matusik [65]. Other studies have achieved higher maximum adsorption capacities, but with different experimental conditions. For instance, Oliveira and Rubio [67] modified zeolite samples (average diameter 25.4 μm) to produce a flocculated barium–zeolite composite, reporting sulfate maximum adsorption as high as 54 mg g^{-1}. Despite achieving this impressive level of sulfate adsorption, this approach produces highly toxic barium residues. On the other hand, Chen and Liu [64] made use of zeolite (sieved with 75 μm standard sieves) modified with CTAB, reaching 38 mg g^{-1} of sulfate maximum

adsorption, but with isotherm construction carried out at 40 °C. Therefore, it is critical to consider experimental details when comparing results across different studies. To obtain further insight into these systems, Freundlich (F), Langmuir (L) and Langmuir–Freundlich (LF) models were applied to determine which model better represented the adsorption mechanism involved (Figure 5). Fitting parameters are presented in Table 3.

Table 3. Adsorption model fit parameters.

Langmuir		**NZ**	**MZ**
$C_{m\text{-}cal}$	(mg g^{-1})	1.48	3.08
K_L	(L mg^{-1})	0.05	0.25
R^2		0.98	1.00
Freundlich		**NZ**	**MZ**
K_F	(mg g^{-1})	0.42	2.2
$1/n_{fads}$		0.21	0.06
R^2		0.94	0.94
Langmuir–Freundlich		**NZ**	**MZ**
$C_{m\text{-}cal}$	(mg g^{-1})	1.74	3.48
K_d		7.45	0.93
N		0.59	0.33
R^2		0.99	1.00

The behavior of the isotherms fit all three adsorption models, as evidenced by the marginal differences between correlation coefficients. This indicates that the relevant adsorption processes do not belong to a single type of process (pure physical or chemical adsorption, for instance). When comparing the R^2 values, the Langmuir–Freundlich model (LF) best fit the adsorption isotherm data. However, maximum adsorption capacity calculated through Langmuir model of 3.08 mg g^{-1} is closer to the experimental value of 3.1 mg g^{-1}, and the model tendency at higher C_{Se} values seems more realistic. Therefore, there are good arguments for selecting both models for the description. In this sense, most sulfate adsorption isotherms adjustment reports found in the literature using similar adsorbents agree that the Langmuir model better represented the experimental data [65–67] compared to the Freundlich model [64]. Authors do not necessarily attempt to use the Langmuir–Freundlich model for fitting their adsorption data, in spite of its applicability to heterogeneous immobilization of ions on solid adsorbents, which involves both Langmuir and Freundlich processes [68].

Analyzing LF parameters, maximum adsorption capacity ($C_{m\text{-}cal}$) on MZ is two times higher than for NZ. As K_d corresponds to the model dissociation constant, its value is a measure if the instability of the interaction between analyte and adsorbent; thus, adsorption interaction over MZ is about eight times stronger than on NZ. Finally, the LF coefficient number, n, represents the cooperativity extent of the process. Since n values are $0 < n < 1$ on both adsorbents, this points to negative cooperativity, meaning that both zeolite-based adsorbents have low affinity for sulfate immobilization and the interaction sites act independently from each other [51,52]. The fact that the three models adjust well to the experimental data means that the adsorption process is a combination of chemical and physical processes. Taking into account that other studies [65] made on surfactant modified zeolites described a reversible adsorption process, it is reasonable to infer that sulfate adsorption on MZ is a partially reversible process. A partially reversible adsorption process is advantageous from the point of view that the composite will maintain the adsorbed sulfate retained while the sulfate concentration and pH values are constant. However, if these conditions change, the adsorbent will liberate sulfate, recovering the adsorbing surface activity for further remediation cycles.

Thus, as explained after the adsorption kinetic results, SO_4^{2-} adsorption capacities on the adsorbents in the present study seem to strongly relate to the surface charge differences

observed at the working pH. MZ corresponds to a zeolite-based adsorbent of sulfate, acting faster and displaying superior adsorption capacities. It should be noted that its adsorption efficiency is lower than other reported materials for sulfate removal [69,70]. However, many of these materials are synthetic (mainly polymers) and not friendly to the environment, so in this sense the product developed in this work has a composition equivalent to soils and sediments with a marginal amount of polycation, reaching a maximum of 0.1 mg per gram of zeolite. MZ represents a low-cost, environmentally friendly, scalable material capable of adsorbing (remediating) sulfate from aqueous solutions with potential applications in the field of copper mining wastewater treatment.

4. Conclusions

The proposed composite between natural zeolite (NZ) samples and a commercial-origin polycationic flocculant (SC-581) resulted in a modified zeolite (MZ) surface with enhanced capacities for sulfate adsorption. Combination of 1 g of zeolite with 0.015 mg of of SC-581 in 25 mL is sufficient to achieve high charge reversion. Evaluation of the ionic strength effect on the adsorption process revealed that KCl concentration should not surpass 0.050 mol L^{-1} to avoid changes in the adsorption process. MZ exhibited double the sulfate adsorption capacities of NZ during adsorption kinetics and isotherms construction. Isotherm data were modeled with three different adsorption models achieving good fitting parameters in all cases. The best correlation is achieved by the Langmuir–Freundlich model, but also seems that the maximum adsorption capacity and the tendency is better described by the Langmuir model.

LF parameters corroborated the enhanced adsorption capacities of MZ compared to NZ, with two times higher maximum adsorption capacities ($C_{m\text{-}cal}$) and an eight times lower dissociation constant (K_d). The differences observed between the adsorption capacity of MZ and NZ can be attributed to distinct surface charge development at working pH (around 5.0). Most of the adsorption takes place by an electrostatic interaction, defining a partially reversible sulfate adsorbent suitable for recycling. Collectively, these data support the further development of MZ for sulfate remediation technologies in wastewater. The methods are simple, low-cost and present low health and environmental risk. Future prospect for this technology is to optimize the adsorption of further anionic pollutants (phosphate, nitrate, arsenate, perchlorate, among others) considering different zeolite-type and polycation combinations.

Author Contributions: C.P.: funding acquisition, methodology, project administration, supervision, writing—review and editing; M.E.: methodology, supervision, writing—review and editing; C.B.: investigation; M.G.: visualization, writing—original draft, writing–review and editing, funding acquisition; L.P.: writing—review and editing. All authors have read and agreed to the published version of the manuscript.

Funding: This work was supported by Proyecto Dicyt–USACH 021742PA (VRIDEI-USACH), Proyecto Fondo Fortalecimiento USA1799, CEDENNA AFB-180001 (Chile), CONICYT PIA/ANILLO ACM 170002 and FONDECYT 11170300.

Data Availability Statement: Data sharing not applicable.

Conflicts of Interest: The authors declare no conflict of interest.

References

1. Statista. Mining—Statistics & Facts. 2018. Available online: https://www.statista.com/topics/1143/mining/ (accessed on 28 October 2020).
2. Harris, J.; McCartor, A. The top ten of the toxic twenty. In *The World's Worst Toxic Pollution Problems*; Blacksmith Institute and Green Cross Switzerland: New York, NY, USA; Zurich, Switzerland, 2011. Available online: http://www.worstpolluted.org (accessed on 28 October 2020).
3. Du, W.; Wang, X.; Chen, G.; Zhang, J.; Slaný, M. Synthesis, property and mechanism analysis of a novel polyhydroxy organic amine shale hydration inhibitor. *Minerals* **2020**, *10*, 128. [CrossRef]

4. Al-Zoubi, H.; Rieger, A.; Steinberger, P.; Pelz, W.; Haseneder, R.; Härtel, G. Optimization study for treatment of acid mine drainage using membrane technology. *Sep. Sci. Technol.* **2010**, *45*, 2004–2016. [CrossRef]
5. Grout, J.A.; Levings, C.D. Effects of acid mine drainage from an abandoned copper mine, Britannia Mines, Howe Sound, British Columbia, Canada, on transplanted blue mussels (Mytilus edulis). *Mar. Environ. Res.* **2001**, *51*, 265–288. [CrossRef]
6. Tait, S.; Clarke, W.P.; Keller, J.; Batstone, D.J. Removal of sulfate from high-strength wastewater by crystallisation. *Water Res.* **2009**, *43*, 762–772. [CrossRef]
7. Baldwin, D.S.; Mitchell, A. Impact of sulfate pollution on anaerobic biogeochemical cycles in a wetland sediment. *Water Res.* **2012**, *46*, 965–974. [CrossRef] [PubMed]
8. Johnson, D.B.; Hallberg, K.B. Acid mine drainage remediation options: A review. *Sci. Total Environ.* **2005**, *338*, 3–14. [CrossRef] [PubMed]
9. Wang, Q.; Shaheen, S.M.; Jiang, Y.; Li, R.; Slaný, M.; Abdelrahman, H.; Kwon, E.; Bolan, N.; Rinklebe, J.; Zhang, Z. Fe/Mn- and P-modified drinking water treatment residuals reduced Cu and Pb phytoavailability and uptake in a mining soil. *J. Hazard. Mater.* **2021**, *403*, 123628. [CrossRef]
10. Du, W.; Slaný, M.; Wang, X.; Chen, G.; Zhang, J. The inhibition property and mechanism of a novel low molecularweight zwitterionic copolymer for improving wellbore stability. *Polymers* **2020**, *12*, 708. [CrossRef]
11. Silva, A.M.; Lima, R.M.F.; Leão, V.A. Mine water treatment with limestone for sulfate removal. *J. Hazard. Mater.* **2012**, *221*, 45–55. [CrossRef]
12. Gacitúa, M.A.; Muñoz, E.; González, B. Bioelectrochemical sulphate reduction on batch reactors: Effect of inoculum-type and applied potential on sulphate consumption and pH. *Bioelectrochemistry* **2018**, *119*, 26–32. [CrossRef]
13. Vujaković, A.; Daković, A.; Lemić, J.; Radosavljević-Mihajlović, A.; Tomasevic-Canovic, M. Adsorption of inorganic anionic contaminants on surfactant modified minerals. *J. Serbian Chem. Soc.* **2003**, *68*, 833–841. [CrossRef]
14. Barczyk, K.; Mozgawa, W.; Król, M. Studies of anions sorption on natural zeolites. *Spectrochim. Acta Part A Mol. Biomol. Spectrosc.* **2014**, *133*, 876–882. [CrossRef] [PubMed]
15. Maree, J.P.; Hlabela, P.; Nengovhela, R.; Geldenhuys, A.J.; Mbhele, N.; Nevhulaudzi, T.; Waanders, F.B. Treatment of mine water for sulphate and metal removal using barium sulphide. *Mine Water Environ.* **2004**, *23*, 195–203. [CrossRef]
16. Weckhuysen, B.M.; Yu, J. Recent advances in zeolite chemistry and catalysis. *Chem. Soc. Rev.* **2015**, *44*, 7022–7024. [CrossRef] [PubMed]
17. Dixon, J.B.; Schulze, D.G. *Soil Mineralogy with Environmental Applications*; Soil Science Society of America Inc.: Madison, WI, USA, 2002; ISBN 0891188398.
18. Motsi, T.; Rowson, N.A.; Simmons, M.J.H. Adsorption of heavy metals from acid mine drainage by natural zeolite. *Int. J. Miner. Process.* **2009**, *92*, 42–48. [CrossRef]
19. Zanin, E.; Scapinello, J.; de Oliveira, M.; Rambo, C.L.; Franscescon, F.; Freitas, L.; de Mello, J.M.M.; Fiori, M.A.; Oliveira, J.V.; Dal Magro, J. Adsorption of heavy metals from wastewater graphic industry using clinoptilolite zeolite as adsorbent. *Process Saf. Environ. Prot.* **2017**, *105*, 194–200. [CrossRef]
20. Kotoulas, A.; Agathou, D.; Triantaphyllidou, I.E.; Tatoulis, T.I.; Akratos, C.S.; Tekerlekopoulou, A.G.; Vayenas, D.V. Zeolite as a potential medium for ammonium recovery and second cheese whey treatment. *Water* **2019**, *11*, 136. [CrossRef]
21. Alshameri, A.; Ibrahim, A.; Assabri, A.M.; Lei, X.; Wang, H.; Yan, C. The investigation into the ammonium removal performance of Yemeni natural zeolite: Modification, ion exchange mechanism, and thermodynamics. *Powder Technol.* **2014**, *258*, 20–31. [CrossRef]
22. Guida, S.; Potter, C.; Jefferson, B.; Soares, A. Preparation and evaluation of zeolites for ammonium removal from municipal wastewater through ion exchange process. *Sci. Rep.* **2020**, *10*, 1–11. [CrossRef]
23. Wang, S.; Peng, Y. Natural zeolites as effective adsorbents in water and wastewater treatment. *Chem. Eng. J.* **2010**, *156*, 11–24. [CrossRef]
24. Gao, L.; Zhang, C.; Sun, Y.; Ma, C. Effect and mechanism of modification treatment on ammonium and phosphate removal by ferric-modified zeolite. *Environ. Technol.* **2019**, *40*, 1959–1968. [CrossRef]
25. Cristiani, C.; Iannicelli-Zubiani, E.M.; Bellotto, M.; Dotelli, G.; Finocchio, E.; Latorrata, S.; Ramis, G.; Stampino, P.G. Capture and release mechanism of La ions by new polyamine-based organoclays: A model system for rare-earths recovery in urban mining process. *J. Environ. Chem. Eng.* **2020**, *9*, 104730. [CrossRef]
26. Kar, S.; Ghosh, S.; Leszczynski, J. Is clay-polycation adsorbent future of the greener society? In silico modeling approach with comprehensive virtual screening. *Chemosphere* **2019**, *220*, 1108–1117. [CrossRef]
27. Gardi, I.; Nir, S.; Mishael, Y.G. Filtration of triazine herbicides by polymer-clay sorbents: Coupling an experimental mechanistic approach with empirical modeling. *Water Res.* **2015**, *70*, 64–73. [CrossRef]
28. Bowman, R.S.; Sullivan, E.J.; Li, Z. Uptake of cations, anions, and nonpolar organic molecules by surfactant-modified clinoptilolite-rich tuff. In *Natural Zeolites for the Third Millennium*; Colella, C., y Mumpton, F.A., Eds.; De Frede Editore: Napoli, Italy, 2000; pp. 287–297.
29. Slaný, M.; Jankovič, Ľ.; Madejová, J. Structural characterization of organo-montmorillonites prepared from a series of primary alkylamines salts: Mid-IR and near-IR study. *Appl. Clay Sci.* **2019**, *176*, 11–20. [CrossRef]
30. Dickson, J.; Conroy, N.A.; Xie, Y.; Powell, B.A.; Seaman, J.C.; Boyanov, M.I.; Kemner, K.M.; Kaplan, D.I. Surfactant-modified siliceous zeolite Y for pertechnetate remediation. *Chem. Eng. J.* **2020**, *402*, 1–11. [CrossRef]

31. An, J.-H.; Dultz, S. Polycation adsorption on montmorillonite: pH and T as decisive factors for the kinetics and mode of chitosan adsorption. *Clay Miner.* **2007**, *42*, 329–339. [CrossRef]
32. Radian, A.; Mishael, Y. Effect of humic acid on pyrene removal from water by polycation-clay mineral composites and activated carbon. *Environ. Sci. Technol.* **2012**, *46*, 6228–6235. [CrossRef]
33. Kamble, S.P.; Mangrulkar, P.A.; Bansiwal, A.K.; Rayalu, S.S. Adsorption of phenol and o-chlorophenol on surface altered fly ash based molecular sieves. *Chem. Eng. J.* **2008**, *138*, 73–83. [CrossRef]
34. Kemira. Información Técnica Serie Superfloc c-500 (c-521-581). Tlaxcala, México. 2017. Available online: http://www.aniq.org.mx/pqta/pdf/Respaldo/Serie%20C500(521-581)%20(HT).pdf (accessed on 28 October 2020).
35. Kemira. Superfloc Floculant and Coagulants. Product Sheet. 2017. Available online: https://www.kemira.com/products/cationic-polyacrylamides/ (accessed on 28 October 2020).
36. Chen, C.L.; Wang, X.K. Influence of pH, soil humic/fulvic acid, ionic strength and foreign ions on sorption of thorium(IV) onto γ-Al_2O_3. *Appl. Geochem.* **2007**, *22*, 436–445. [CrossRef]
37. Verbinnen, B.; Block, C.; Hannes, D.; Lievens, P.; Vaclavikova, M.; Stefusova, K.; Gallios, G.; Vandecasteele, C. Removal of Molybdate Anions from Water by Adsorption on Zeolite-Supported Magnetite. *Water Environ. Res.* **2012**, *84*, 753–760. [CrossRef]
38. van Hooff, J.H.C.; Roelofsen, J.W. *Introduction to Zeolite Science and Practice*; Stud. Surf. Sci. Catal.; Van Bekkum, H., Flanigen, E.M., Jansen, J.C., Eds.; Elsevier: Amsterdam, The Netherlands, 1991; Volume 58, pp. 242–282.
39. Pizarro, C.; Rubio, M.A.; Escudey, M.; Albornoz, M.F.; Muñoz, D.; Denardin, J.; Fabris, J.D. Nanomagnetite-zeolite composites in the removal of arsenate from aqueous systems. *J. Braz. Chem. Soc.* **2015**, *26*, 1887–1896. [CrossRef]
40. Jackson, M.L. *Soil Chemical Analysis: Advanced Course*; Parallel Press, University of Wisconsin-Madison-Libraries: Madison, WI, USA, 2005; p. 101.
41. Soil Survey Staff, United States Department of Agriculture. *Claves Para la Taxonomía de Los Suelos*, 10th ed.; Servicio de conservación de Recursos Naturales; Departamento de Agricultura de los Estados Unidos: Washington, DC, USA, 2006; pp. 77–96.
42. Wu, W.; Palmarin, M.J.; Young, S. Poly(dimethylamine-co-epichlorohydrin) as an alternative to alum for the demulsification of commercial dishwasher wastewater. *Sep. Purif. Technol.* **2018**, *195*, 281–287. [CrossRef]
43. Carter, D.L.; Heilman, M.D.; Gonzales, C.L. Ethylene glycol monoethyl ether for determining surface area of silicate minerals. *Soil Sci.* **1965**, *100*, 356–360. [CrossRef]
44. Brunauer, S.; Emmett, P.H.; Teller, E. Adsorption of Gases in Multimolecular Layers. *J. Am. Chem. Soc.* **1938**, *60*, 309–319. [CrossRef]
45. Jackson, M.L. *Soil Chemical Analysis, Advanced Course*, 2nd ed.; 11th printing; Department of Soil Science, University of Wisconsin–Madison, 1525 Observatory Drive: Madison, WI, USA, 1985.
46. Hunter, R.J. *Zeta Potential in Colloid Science. Principles and Applications*; Academic Press: London, UK, 1983.
47. Evangelou, V.P. *Environmental Soil and Water Chemistry: Principles and Applications*, 1st ed.; Wiley-Interscience: Lexington, KY, USA, 1998.
48. Hsini, A.; Naciri, Y.; Benafqir, M.; Ajmal, Z.; Aarab, N.; Laabd, M.; Navío, J.A.; Puga, F.; Boukherroub, R.; Bakiz, B.; et al. Facile synthesis and characterization of a novel 1,2,4,5-benzene tetracarboxylic acid doped polyaniline@zinc phosphate nanocomposite for highly efficient removal of hazardous hexavalent chromium ions from water. *J. Colloid Interface Sci.* **2021**, *585*, 560–573. [CrossRef]
49. Ho, Y.S. Review of second-order models for adsorption systems. *J. Hazard. Mater.* **2006**, *136*, 681–689. [CrossRef]
50. Hsini, A.; Naciri, Y.; Laabd, M.; El Ouardi, M.; Ajmal, Z.; Lakhmiri, R.; Boukherroub, R.; Albourine, A. Synthesis and characterization of arginine-doped polyaniline/walnut shell hybrid composite with superior clean-up ability for chromium (VI) from aqueous media: Equilibrium, reusability and process optimization. *J. Mol. Liq.* **2020**, *316*, 113832. [CrossRef]
51. Andrade, J.D. *Surface and Interfacial Aspects of Biomedical Polymer*; Plenum Press: New York, NY, USA, 1995; Volume 2.
52. Sharma, S.; Agarwal, G.P. Interactions of proteins with immobilized metal ions: A comparative analysis using various isotherm models. *Anal. Biochem.* **2001**, *288*, 126–140. [CrossRef] [PubMed]
53. Giles, C.H.; Smith, D.; Huitson, A. A general treatment and classification of the solute adsorption isotherm. I. Theoretical. *J. Colloid Interface Sci.* **1974**, *47*, 755–765. [CrossRef]
54. Carvajal-Bernal, A.M.; Gómez-Granados, F.; Giraldo, L.; Moreno-Piraján, J.C. Calorimetric evaluation of activated carbons modified for phenol and 2,4-dinitrophenol adsorption. *Adsorption* **2016**, *22*, 13–21. [CrossRef]
55. Rand, M.C.; Greenberg, A.E.; Taras, M.J. *Standard Methods for the Examination of Water and Wastewater*, 14th ed.; APHA (American Public Health Association); AWWA (American Water Works Association); WEF (Water Environment Federation): Washington, DC, USA, 1975; Method 427C; p. 496.
56. Escudey, M.; Gil-Llambias, F. Effect of cation and anion adsorption on the electrophoretic behavior of MoO3/γ-AIO3 catalysts. *J. Colloid Interface Sci.* **1985**, *107*, 272–275. [CrossRef]
57. Arancibia-Miranda, N.; Silva-Yumi, J.; Escudey, M. Effect of cations in the background electrolyte on the adsorption kinetics of copper and cadmium and the isoelectric point of imogolite. *J. Hazard. Mater.* **2015**, *299*, 675–684. [CrossRef]
58. Smets, G.; Hesbain, A.M. Hydrolysis of polyacrylamide and acrylic acid–acrylamide copolymers. *J. Polym. Sci.* **1959**, *40*, 217–226. [CrossRef]
59. Pubchem. Compound Summary for CAS Nº 42751-79-1. 2017. Available online: https://pubchem.ncbi.nlm.nih.gov/compound/115172#section=Top (accessed on 28 October 2020).

60. Mondal, P.; Tran, A.T.K.; Van der Bruggen, B. Removal of As(V) from simulated groundwater using forward osmosis: Effect of competing and coexisting solutes. *Desalination* **2014**, *348*, 33–38. [CrossRef]
61. Wang, L.; Zhang, J.; Zhao, R.; Li, Y.; Li, C.; Zhang, C. Adsorption of Pb(II) on activated carbon prepared from Polygonum orientale Linn.: Kinetics, isotherms, pH, and ionic strength studies. *Bioresour. Technol.* **2010**, *101*, 5808–5814. [CrossRef]
62. Yang, X.; Yang, S.; Yang, S.; Hu, J.; Tan, X.; Wang, X. Effect of pH, ionic strength and temperature on sorption of Pb(II) on NKF-6 zeolite studied by batch technique. *Chem. Eng. J.* **2011**, *168*, 86–93. [CrossRef]
63. Worch, E. *Adsorption Technology in Water Treatment: Fundamentals, Processes, and Modeling*; Walter de Gruyter, Hubert and Co, GmbH and Co: Gottigen, Germany, 2012; ISBN 3110240238.
64. Chen, W.; Liu, H.C. Adsorption of sulfate in aqueous solutions by organo-nano-clay: Adsorption equilibrium and kinetic studies. *J. Cent. South Univ.* **2014**, *21*, 1974–1981. [CrossRef]
65. Matusik, J. Arsenate, orthophosphate, sulfate, and nitrate sorption equilibria and kinetics for halloysite and kaolinites with an induced positive charge. *Chem. Eng. J.* **2014**, *246*, 244–253. [CrossRef]
66. Li, Z.; Zhang, Y. Use of surfactant-modified zeolite to carry and slowly release sulfate. *Desalin. Water Treat.* **2010**, *21*, 73–78. [CrossRef]
67. Oliveira, C.R.; Rubio, J. New basis for adsorption of ionic pollutants onto modified zeolites. *Miner. Eng.* **2007**, *20*, 552–558. [CrossRef]
68. Jeppu, G.P.; Clement, T.P. A modified Langmuir-Freundlich isotherm model for simulating pH-dependent adsorption effects. *J. Contam. Hydrol.* **2012**, *129–130*, 46–53. [CrossRef] [PubMed]
69. Sang, P.L.; Wang, Y.Y.; Zhang, L.Y.; Chai, L.Y.; Wang, H.Y. Effective adsorption of sulfate ions with poly(m-phenylenediamine) in aqueous solution and its adsorption mechanism. *Trans. Nonferrous Met. Soc. China* **2013**, *23*, 243–252. [CrossRef]
70. Sadeghalvad, B.; Khorshidi, N.; Azadmehr, A.; Sillanpää, M. Sorption, mechanism, and behavior of sulfate on various adsorbents: A critical review. *Chemosphere* **2021**, *263*, 128064. [CrossRef]